JOURNAL OF SOLID STATE CHEMISTRY **121,** 190–196 (1996)
ARTICLE NO. 0027

Changes of Crystalline Phase and Catalytic Properties by Cation Substitution in Mirror Plane of Hexaaluminate Compounds

H. Inoue, K. Sekizawa, K. Eguchi, and H. Arai[1]

Department of Materials Science and Technology, Graduate School of Engineering Sciences, Kyushu University 39, 6-1, Kasuga-koen, Kasuga, Fukuoka 816, Japan

Received May 30, 1995; accepted September 13, 1995

Mn-substituted hexaaluminate compounds have been investigated as catalysts for high temperature combustion above 1000°C. In this study, changes of crystalline phase and catalytic properties of $Sr_{1-x}Ln_xMnAl_{11}O_{19-\alpha}$ (Ln = Pr, Nd, Sm, Gd) were investigated. Two kinds of hexaaluminate phases existed as equilibrium phases in the unsubstituted sample, the *Ln* ions were preferentially soluble in one of these phases. Accompanied with the dissolution, unequilibrium $LnAlO_3$ phase was sometimes formed for high *x* samples. The amount of this phase decreases with an increase in temperature and/or ionic radius of *Ln*. The surface area of the samples generally decreased with increasing extent of *Ln* substitution. Catalytic activity for methane combustion at low conversion level was improved by the substitution.

INTRODUCTION

A great number of combustors have produced vast amounts of energy for industry and living uses by flame combustion of hydrocarbon fuel. As the temperature of flame combustion is raised in order to attain high efficiency, nitrogen oxide emission becomes significant enough to cause atmospheric pollution, especially acid rain. In order to suppress the nitrogen oxide emission from combustors, the catalytic combustion method has attracted special interest recently (1–4). Catalytic combustion can be classified from the operation temperature into low, middle, and high temperature types. Among them, the information on high temperature catalytic combustion above 1000°C is insufficient because of a lack of catalyst materials in use at such temperatures.

It was found previously that $BaO \cdot 6Al_2O_3$ prepared by alkoxides hydrolysis can maintain a surface area of about 10 m^2g^{-1}, which is higher than Al_2O_3, even at 1600°C. The high thermal resistance of this compound is quite useful for high temperature catalyst supports (5). Hexaaluminate compounds containing alkali, alkaline earth, or rare earth metals have β-Al_2O_3 or magnetoplumbite-type crystal structure as shown in Fig. 1 (6–8). This structure consists of alternate stacking of a spinel block with close packed oxide ions and a mirror plane with the large cation along the *c* axis. β-Al_2O_3 and magnetoplumbite-type structures have different atomic arrangements in the mirror plane from each other. Depending on an ionic radius and/or a valence of the mirror plane cation (9), a hexaaluminate compound possesses one of these structural types. In the previous studies, it has been revealed that oxygen diffusion along the $\perp c$ direction is faster in a hexaaluminate crystal than that along the $/\!/ c$ direction. Therefore, mirror planes are expected as a preferential diffusion route of oxide ion (10, 11). The crystal growth along the $/\!/ c$ direction should be, therefore, suppressed to crystallize in thin plate-like morphology. Due to this anisotropic crystal shape and mass diffusion, a large surface area can be maintained at high temperatures.

Partial cation substitution by some transition metals (Co, Ni, Cr, Fe, and Mn) for the Al site in the hexaaluminate lattice provides high catalytic activity for the oxidation of hydrocarbon. The partial substitution of Mn leads to the highest catalytic activity (12). The catalytic activity, which is brought about by the redox cycle of Mn, can be further improved by partial substitution for the mirror plane cation by the cation with approximately equal ionic radius to that of host cation (13). Mn and La ions in the strontium hexaaluminate lattice occupy the Al and Sr sites, respectively, as expressed by $Sr_{0.8}La_{0.2}MnAl_{11}O_{19-\alpha}$, which is attractive as a high temperature combustion catalyst with its high catalytic activity and surface area at high temperatures. In the present study, crystalline phase, surface area, and catalytic activity for methane combustion of $Sr_{1-x}Ln_xMnAl_{11}O_{19-\alpha}$ (Ln = Ce, Pr, Nd, Sm, and Gd) were investigated in order to improve thermal resistance and catalytic activity. Particularly, changes of the crystalline phase of Pr-substituted sample by cation substitution was observed in detail as a function of calcination temperature and composition.

[1] To whom correspondence should be addressed.

0022-4596/96 $12.00

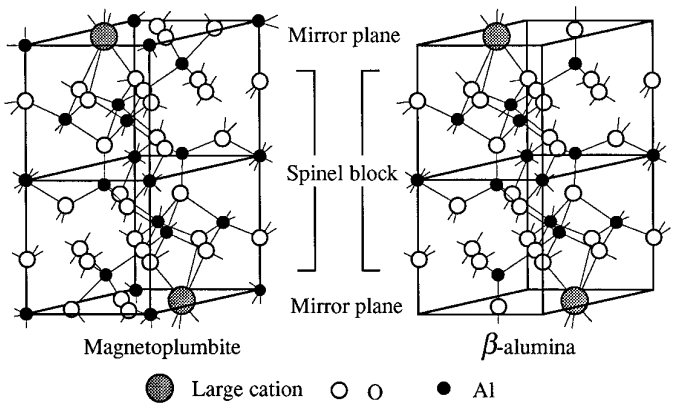

FIG. 1. Crystal structure of magnetoplumbite and β-alumina.

EXPERIMENTAL

Sample Preparation

Manganese-substituted hexaaluminates $Sr_{1-x}Ln_xMnAl_{11}O_{19-\alpha}$ (Ln = Ce, Pr, Nd, Sm, Gd; x = 0, 0.2, 0.4, 0.6, 1.0) were prepared by hydrolysis of composite metal alkoxides. Calculated amounts of Sr metal (98%, Kishida Reagents Chemicals) and $Al(OC_3H_7)_3$ (99%, Kishida Reagents Chemicals) were stirred in 2-propanol (99.5%, Kishida Reagents Chemicals) until dissolution was completed and kept at about 80°C for 3 hr in a dry N_2 atmosphere. After a mixed aqueous solution of manganese nitrate and lanthanum nitrate was dropped to the alcoholic solution with the molar ratio of water/metal alkoxyl group = 1, the resulting precipitate thus formed with gelation was aged for several hours and evaporated to dryness. Then the powder was thermally decomposed at 500°C and subsequently calcined in air.

Measurements of Crystalline Phase

The thermally decomposed precursor of $Sr_{1-x}Pr_xMnAl_{11}O_{19-\alpha}$ (x = 0, 0.2, and 0.4) was calcined for 5 hr at 1200, 1400, and 1600°C in air. The crystal structures of calcined samples were determined by X-ray diffraction (Rigaku, RINT1400) with Cu$K\alpha$ radiation. The sample calcined at 1400°C was observed by a JEM 2000FX transmission electron microscope (TEM) operated at 200 kV. The energy-dispersive X-ray (EDX) spectra were recorded for several hexaaluminate crystallites by using Tracor Northern TN2000 installed on the microscope. The concentration ratio of components was calculated by using the equation from the spectra (14),

$$C_A/C_B = k_{AB}I_A/I_B,$$

where C_A and C_B are the concentration (wt%), I_A and I_B are the characteristic X-ray intensities of element A and B in the analyzed volume, respectively, and k_{AB} is a proportionality factor. Values of k_{AB} used for calculation were k_{SrAl} = 3.0502, k_{PrAl} = 2.6779, k_{MnAl} = 1.2882. The spectrum lines of Sr$K\alpha$ (13.84–14.30 keV), Pr$L\alpha$ (4.84–5.18 keV), Mn$K\alpha$ (5.74–6.00 keV), and Al$K\alpha$ (1.38–1.58 keV) were used for calculation. The correction for overlapping peaks and a background was performed by fitting the obtained spectra using standard spectra measured respectively for $SrCO_3$, Pr_6O_{11}, metallic Mn, and Al.

Measurements of Catalytic Properties

The surface areas of calcined powders were determined by the BET method using nitrogen adsorption at 77 K. Catalytic activities were measured in a conventional flow system under atmospheric pressure. Catalysts were fixed in a quartz reactor by packing alumina beads at both ends of the catalysts bed. A gaseous mixture of methane (1 vol%) and air (99 vol%) was fed to the catalyst bed at a flow rate of 48,000 cm^3hr^{-1} (space velocity = 48,000 hr^{-1}). The methane conversion in the effluent gas was analyzed by on-line gas chromatography.

RESULTS AND DISCUSSION

Crystalline Phase of Samples Calcined at 1200°C

In our previous studies, Mn-substituted hexaaluminate samples with various mirror plane cations, $A_{0.8}A'_{0.2}MnAl_{11}O_{19-\alpha}$ (A = Ba, Sr; A' = K, Ca, Sr, La), prepared by hydrolysis of metal alkoxides were investigated as the catalysts for combustion of methane after calcination at 1300°C for 5 hr (13). The catalytic activities were markedly improved in the low-conversion region when the combination of A and A' is Ba and K or Sr and La. In both cases, the ionic radii of A and A' are very close but the valences are different. The ratio of ionic radii, $R_{i.r.}$ defined as follows was 0.93 or 0.96, respectively, for Ba–K and Sr–La couples.

$$R_{i.r.} = \text{ionic radius of } A'/\text{ionic radius of } A$$

$Ba_{0.8}K_{0.2}MnAl_{11}O_{19-\alpha}$ and $Sr_{0.8}La_{0.2}MnAl_{11}O_{19-\alpha}$ can be generally obtained as single phases of $BaAl_{12}O_{19}$-type β-Al_2O_3 structure and a single phase of $SrAl_{12}O_{19}$-type magnetoplumbite-type structure, respectively. In this study, Sr and Ln (Ce, Pr, Nd, Sm, or Gd) with close ionic radius to Sr, were respectively chosen as A and A' cations.

Table 1 shows the crystalline phase of $Sr_{1-x}Ln_xMnAl_{11}O_{19-\alpha}$ (x = 0, 0.4, and 1.0) determined by X-ray diffraction. In XRD pattern of unsubstituted sample (x = 0), strong peaks assigned to $SrAl_{12}O_{19}$, and weak peaks assigned to $SrAl_4O_7$ appeared. Most of diffraction peaks assigned to $SrAl_{12}O_{19}$ were observed as doublets.

In the case of Ce-substituted sample (Ln = Ce), the CeO_2 phase existed as an impurity in addition to the

TABLE 1
Surface Area and Crystalline Phase of Sr–Hexaaluminates Substituted by Lanthanide Cation in the Mirror Plane Calcined at 1200°C

Sample	$R_{i.r.}$[a]	Surface area (m^2g^{-1})	Crystalline phase[b]	I_p/I_h[c]
$SrMnAl_{11}O_{19-\alpha}$	—	20.8	*SA*6(2phase) + *SA*	—
$Sr_{0.6}Ce_{0.4}MnAl_{11}O_{19-\alpha}$	0.93	10.7	*SA*6 + CeO_2	—
$Sr_{0.6}Pr_{0.4}MnAl_{11}O_{19-\alpha}$	0.91	14.9	*SA*6 + *P*	11
$Sr_{0.6}Nd_{0.4}MnAl_{11}O_{19-\alpha}$	0.91	18.6	*SA*6 + *P*	21
$Sr_{0.6}Sm_{0.4}MnAl_{11}O_{19-\alpha}$	0.89	15.3	*SA*6 + *P*	25
$Sr_{0.6}Gd_{0.4}MnAl_{11}O_{19-\alpha}$	0.87	16.8	*SA*6 + *P*	22
$PrMnAl_{11}O_{19-\alpha}$	—	12.5	*SA*6 + *P* + α	18
$NdMnAl_{11}O_{19-\alpha}$	—	11.1	*SA*6 + *P* + α	32
$SmMnAl_{11}O_{19-\alpha}$	—	6.3	*SA*6 + *P* + α	48
$GdMnAl_{11}O_{19-\alpha}$	—	6.6	*P* + α	—

[a] Ratio of ionic radii between Sr and Ln in $Sr_{0.6}Ln_{0.4}MnAl_{11}O_{19-\alpha}$.
[b] *SA*6 = $SrAl_{12}O_{19-\alpha}$, *SA* = $SrAl_4O_7$, *P* = perovskite-type $LnAlO_3$, α = α-Al_2O_3.
[c] Intensity ratio of $LnAlO_3$ (100)/hexaaluminate (110).

$SrAl_{12}O_{19}$ phase. The intensity of the CeO_2 phase increased with an increase in substitution (x = 0.1–0.4). Ionic radius of Ce^{3+} is 1.18 Å and $R_{i.r.}$ is 0.93. It is reported by Iyi *et al.* (9) that the only mono-, di-, and trivalent ions with ionic radii above 1.10 Å can be accommodated in the mirror plane of the hexaaluminate compounds. Although this value implies high solubility of Ce in the lattice, Ce was almost insoluble in the hexaaluminate lattice, supposedly because of tetravalent Ce ions. This result agreed with the experimental data reported by Yamashita *et al.* (15). The Ce-substituted sample was, therefore, excluded from the following discussion.

Other lanthanide cations were soluble in the hexaaluminate lattice, and their X-ray diffraction patterns were similar to each other. As for the sample at x = 0.4, the hexaaluminate phase and $LnAlO_3$ perovskite phase coexisted. As the amount of substitution increased from x = 0.4 to x = 0.6, the diffraction peaks of the perovskite phase were intensified and a weak α-Al_2O_3 line was also observed. When Pr, Nd, and Sm were wholly substituted (x = 1.0), a *Ln*–hexaaluminate phase was formed. In contrast, the Gd–hexaaluminate lines were so weak that they were hidden in the background in the Gd-substituted sample at x = 1.0. The main crystalline phases in this sample were perovskite-type $GdAlO_3$ and α-Al_2O_3. Here we defined a relative peak intensity, I_p/I_h, of impurity $LnAlO_3$ phase to that of hexaaluminate.

$$I_p/I_h = \text{intensity of } LnAlO_3\ (100)/\text{intensity of } SrAl_{12}O_{19}\ (110)$$

The I_p/I_h value tended to increase with a decrease in $R_{i.r.}$ (Table 1).

Generally the hydrolysis of metal alkoxides used for the preparation of the present samples is effective in achieving homogeneous dispersion of each element at the atomic level. Even though the sample was prepared by hydrolysis of metal alkoxides, the unequilibrium perovskite phase coexisted with the hexaaluminate phase, as shown in Table 1. The formation of the cation-substituted hexaaluminate simultaneously accompanies the formation of the perovskite phases. Although lanthanide cations with ionic radii close to that of the host cation (Sr) were selected as the substituent, partial substitution of ions with smaller $R_{i.r.}$ resulted in larger content of the impurity phase.

Crystalline Phases of Samples Calcined at Various Temperatures

The crystalline phases and their ratio strongly depended on x. The unequilibrium perovskite phase became abundant as $R_{i.r.}$ value became small. Detailed observation was made for the drastic change of the relative amount of two kinds of hexaaluminate phases at x = 0–0.4. Since the phases formed by substitution were almost similar irrespective of the kind of *Ln*, Pr was selected as a substituent and is expected to be the most soluble because of its close ionic radius to Sr.

XRD patterns of $Sr_{1-x}Pr_xMnAl_{11}O_{19-\alpha}$ (x = 0–1.0) calcined at 1200, 1400, and 1600°C are shown in Figs. 2, 3, and 4, respectively. The unsubstituted sample (x = 0) calcined at 1200°C consisted of two kinds of hexaaluminate phases and $SrAl_4O_7$ as previously described. The peak intensities of the two hexaaluminate phases were approximately the same. Hereinafter the phases that appeared at lower and higher diffraction angles are expressed as phase *A* and phase *B*, respectively.

After calcination at 1200°C, the relative amount of phase *A* decreased in comparison with phase *B* at x = 0.2 and

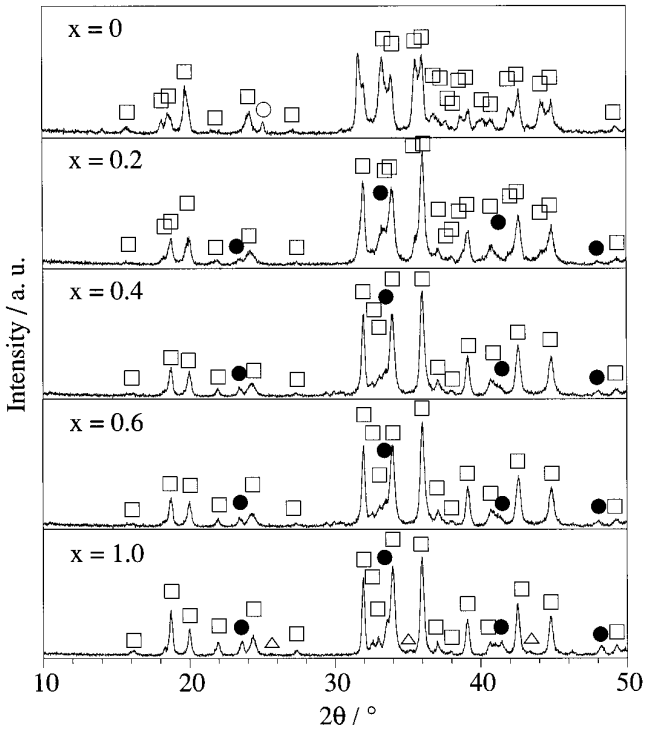

FIG. 2. X-ray diffraction patterns of $Sr_{1-x}Pr_xMnAl_{11}O_{19-\alpha}$ calcined at 1200°C. □ $SrAl_{12}O_{19}$ (⊞ doublet), ○ $SrAl_4O_7$, ● $PrAlO_3$, △ α-Al_2O_3.

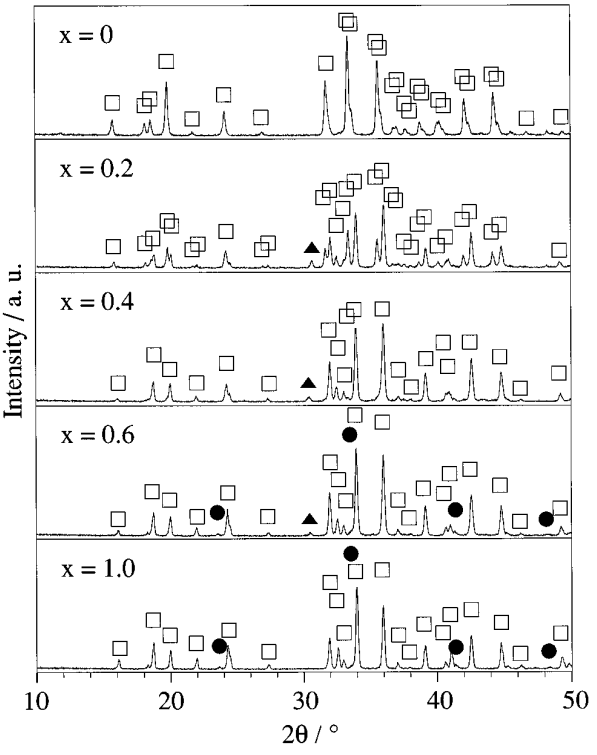

FIG. 4. X-ray diffraction patterns of $Sr_{1-x}Pr_xMnAl_{11}O_{19-\alpha}$ calcined at 1600°C. □ $SrAl_{12}O_{19}$ (⊞ doublet), ▲ characteristic peak of $Sr_3Al_{32}O_{51}$, ● $PrAlO_3$.

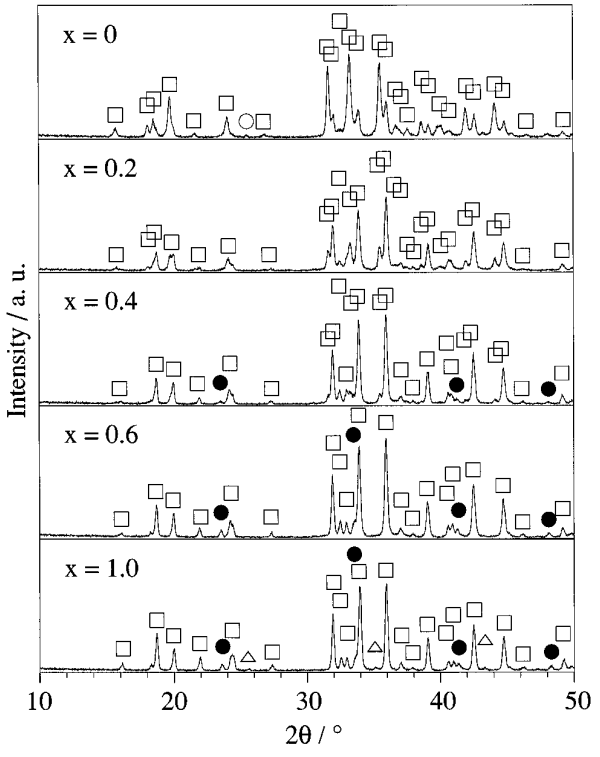

FIG. 3. X-ray diffraction patterns of $Sr_{1-x}Pr_xMnAl_{11}O_{19-\alpha}$ calcined at 1400°C. □ $SrAl_{12}O_{19}$ (⊞ doublet), ○ $SrAl_4O_7$, ● $PrAlO_3$, △ α-Al_2O_3.

$PrAlO_3$ was also observed. Ionic radius of Pr is 1.16 Å in the trivalent state. Iyi *et al.* (9) have reported that Pr is quite soluble as a mirror plane cation of the magneto-plumbite-type hexaaluminate. Therefore, it is suggested that the perovskite type oxide, $PrAlO_3$, is an unequilibrium phase which should disappear after prolonged calcination. The formation of the lanthanide (Y, Nd, Pr, Sm, Gd, or Dy) perovskite compounds is kinetically easy. With a further increase in x up to $x = 1.0$, the diffraction peak of $PrAlO_3$ was intensified.

In the case of $Sr_{1-x}Pr_xMnAl_{11}O_{19-\alpha}$ calcined at 1400°C, $PrAlO_3$ did not exist at $x = 0.2$. However, above $x = 0.4$, the unequilibrium $PrAlO_3$ phase was formed, as well as in the case of calcination at 1200°C. The peak intensity of this perovskite phase increased with an increase in x. Although phase A and B had almost equal diffraction peak intensity at $x = 0$ after calcination at 1200°C, the peak of phase A was stronger than that of phase B at $x = 0$ after calcination at 1400°C. In XRD patterns of $Sr_{1-x}Pr_xMnAl_{11}O_{19-\alpha}$, phase A was absent at $x = 0.4$ after calcination at 1200°C, whereas this phase could be observed at $x \leqq 0.4$ after calcination at 1400°C. It is expected that phase A is more stable than phase B at high temperatures.

When $Sr_{1-x}Pr_xMnAl_{11}O_{19-\alpha}$ were calcined at 1600°C, $PrAlO_3$ was observed only at high Pr concentration ($x =$

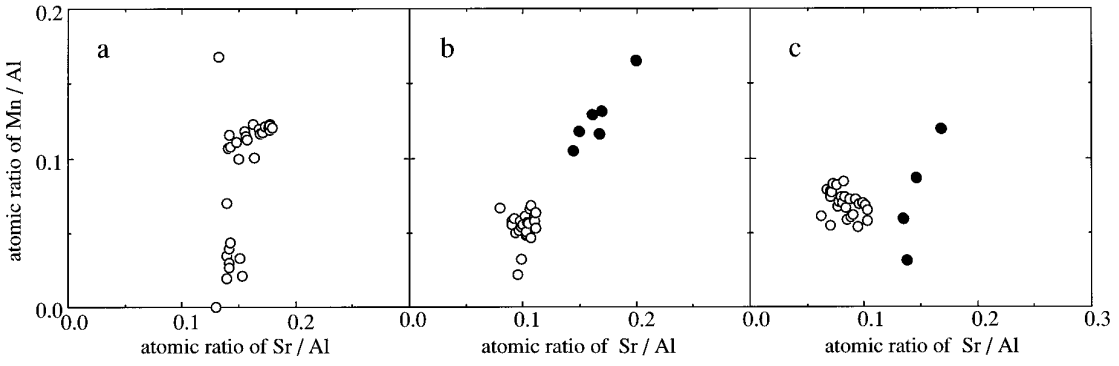

FIG. 5. Chemical composition of $Sr_{1-x}Pr_xMnAl_{11}O_{19-\alpha}$ crystallite, (a) $x = 0$, (b) $x = 0.2$, (c) $x = 0.4$, ● Pr-poor crystallite.

0.6 and 1.0) since high calcination temperature facilitated the dissolution of Pr in the hexaaluminate phases. The peak of phase *A* became even more strong than that of phase *B* at $x = 0$ after calcination at 1600°C. The coexistence of two hexaaluminate phases was seen only at $x \leqq 0.2$. With increasing x, phase *B* became dominant in the sample as well as those calcined at lower temperatures. A characteristic peak for $x = 0.2$, 0.4, and 0.6 at $2\theta =$ ca. 30° could be assigned to $Sr_3Al_{32}O_{51}$ with a hexagonal structure. This compound is not described in the phase diagram of the $SrO–Al_2O_3$ system (16). The composition can be rewritten as $Sr_{1.125}Al_{12}O_{19.125}$. It is expected that $Sr_{1.125}Al_{12}O_{19.125}$ is a hexaaluminate phase in which excess cations existed in the mirror plane in comparison with the spinel block. Most of the peaks of this compound appeared at the same diffraction angles as those of $SrAl_{12}O_{19}$.

Chemical Composition of the Crystallite

XRD measurements indicated that the substitution of Pr brings about preferential formation of phase *B*. Considering the ionic size, the lattice is expected to shrink as Pr is substituted for Sr. In order to confirm the preferential substitution of Pr into phase *B*, the chemical composition of each crystallite in $Sr_{1-x}Pr_xMnAl_{11}O_{19-\alpha}$ ($x = 0$, 0.2, and 0.4) calcined at 1400°C was analyzed by EDX as shown in Figs. 5a–5c. XRD patterns of three samples used in this analysis are shown in Fig. 3, in which changes in amount of the two kinds of hexaaluminate phases were discernible.

The crystallites at $x = 0$ were separated from their composition into Mn-rich and Mn-poor groups (Fig. 5a). This result agreed with the previous report (13). The Mn-rich crystallites were larger in number than the others. It is thought that the Mn-rich and Mn-poor crystallites correspond to phase *A* and phase *B*, respectively, judging from the ratio of diffraction peak intensity in Fig. 3.

As shown in Fig. 5b, the number of the Mn-rich crystallite in the sample at $x = 0.2$ was significantly smaller than in the sample at $x = 0$ (Fig. 5a). This indicates that phase *A* decreased and phase *B* increased with increasing x in agreement with XRD results. The EDX analysis obviously indicated that the crystallites are classified into two groups with different Pr contents. The Pr-poor crystallites were denoted in the figure by the closed circles. The Sr/Al ratio decreased obviously only for phase *B* with increasing x. This decrease suggests that Pr ions preferentially substituted in the hexaaluminate crystal with poor Mn concentration. In contrast, the Sr/Al ratio of Mn-rich crystallites was almost unchanged irrespective of x. The increase of Mn/Al ratio in phase *B* with x results from charge compensation. The excessive charge accompanied with the substitution of Pr^{3+} for the Sr^{2+} site may be compensated by introducing divalent Mn at the Al site of the spinel block.

At $x = 0.4$ the number of Mn-rich crystallites decreased and the Mn-poor crystallites tended to possess unique Mn/Al and Sr/Al ratios as shown in Fig. 5c. The Sr concentration of these crystallites decreased naturally by Pr substitution. The Mn concentration of these crystallites in Fig. 5c further increased in comparison with that in Fig. 5b. These results indicate that the high solubility of Pr into hexaaluminate requires the increase in concentration of Mn. The Mn concentration in phase *B* is supposed to be close to the nominal composition of $Sr_{0.6}Pr_{0.4}MnAl_{11}O_{19-\alpha}$.

Surface Area of $Sr_{1-x}Ln_xMnAl_{11}O_{19-\alpha}$

At the inlet of a catalytic combustor, the kinetics of the chemical reaction at the surface of the catalyst is most important in controlling the rate of combustion because of the low reaction temperature. The reaction rate is enhanced with a rise in temperature so that the overall process is limited by the rate of mass transport to the surface. As the exothermic surface reaction proceeds further, the catalyst temperature rises to initiate the radical reaction at the down stream within the catalyst bed, where the gas-phase reactions concurrently proceed with the catalytic reactions to complete the combustion. In the heavy load catalytic combustors with a fast gaseous flow at high tem-

TABLE 2
Surface Area of $Sr_{1-x}Ln_xMnAl_{11}O_{19-\alpha}$ after Calcination at 1200°C

	Surface area ($m^2\ g^{-1}$)				
Ln	$x = 0$	$x = 0.2$	$x = 0.4$	$x = 0.6$	$x = 1.0$
Ce	20.8	13.4	10.7	—	—
Pr	20.8	20.6	14.9	17.7	12.5
Nd	20.8	17.8	18.6	16.9	11.1
Sm	20.8	17.7	15.3	13.9	6.3
Gd	20.8	17.6	16.8	13.7	6.6

peratures, e.g., gas turbine and boiler, combination of both heterogeneous and homogeneous combustion of fuel is required. The rate of heterogeneous reaction on a catalyst surface is regulated by mass transport to the catalyst surface in a high-temperature region. The radical which induces the homogeneous gas phase combustion is generated on the catalyst surface. Therefore, the large surface area of the catalyst is naturally desirable.

The specific surface area of $Sr_{1-x}Ln_xMnAl_{11}O_{19-\alpha}$ after calcination for 5 hr at 1200°C is summarized in Table 2. The specific surface area of every substituted sample was smaller than that of unsubstituted sample ($x = 0$). Among them, the specific surface area of the Ce-substituted sample was markedly smaller than those of other lanthanide-substituted samples, probably because of the coexisting CeO_2 phase. In the Sm- and Gd-substituted samples, the specific surface area decreased with increasing x. In the case of Pr- and Nd-substituted samples, the specific surface area possessed a maximum or minimum value with x. The XRD intensity of the impurity phase, $LnAlO_3$, increased monotonically with an increase in x. These changes in specific surface area did not result only from the coexisting impurity phase, but also from the change of sintering character and/or the low crystallization temperature of these samples.

Surface Area of $Sr_{1-x}Pr_xMnAl_{11}O_{19-\alpha}$ Calcined at 1400°C

The specific surface area of $Sr_{1-x}Pr_xMnAl_{11}O_{19-\alpha}$ calcined at 1400°C for 5 hr was measured by the BET method as a function of x (Fig. 6) to find the relation with the crystalline phase in Fig. 3. The specific surface area decreased with an increase in x at $x \leqq 0.6$. It is probable that this decrease in specific surface area corresponds to the decrease in peak intensity of phase *A* in Fig. 3. In other words, Pr-rich phase *B* has a smaller specific surface area than Pr-poor phase *A*. The specific surface area of the sample corresponded well to the aspect ratio (width/thickness) of the crystallite (13). Therefore, the crystallite of phase *B* appears to possess a smaller aspect ratio than phase *A*.

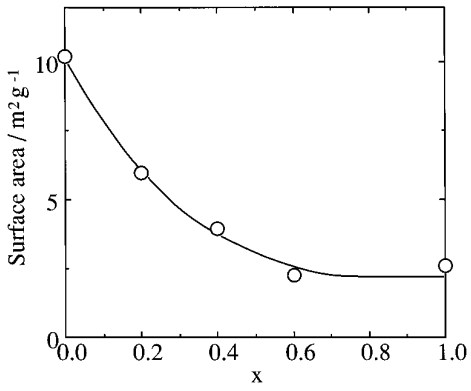

FIG. 6. Dependence of surface area of $Sr_{1-x}Pr_xMnAl_{11}O_{19-\alpha}$ with x after calcination at 1400°C.

Catalytic Activities on CH_4 Combustion

The catalytic activities for CH_4 combustion over $Sr_{1-x}Ln_xMnAl_{11}O_{19-\alpha}$ (*Ln* = Pr, Nd, Sm, and Gd; $x = 0$, 0.2, 0.4, 0.6, and 1.0) calcined at 1200°C were investigated as summarized in Table 3. The Ce-substituted sample was excluded because of its small solubility in the hexaaluminate lattice. In this table, $T_{10\%}$ and $T_{90\%}$ represent the temperatures at which methane conversion of 10% and 90% are attained, respectively. For $T_{10\%}$, the reaction rate was greatly influenced by the catalytic activity at the surface at the low conversion level. However, the reaction rate at high conversion level (90%) was strongly influenced by the mass transport to the surface of the catalyst. As shown in Table 3, $T_{10\%}$ values of the partially substituted samples ($x \neq 0$), except for the sample of *Ln* = Sm at $x = 1.0$, was lower than that of unsubstituted sample. Although the catalytic activity was generally improved by *Ln* substitution, no large difference in catalytic activity could be seen among samples with different lanthanide cations and with different x. The sample which attained the highest catalytic activity was $Sr_{0.6}Nd_{0.4}MnAl_{11}O_{19-\alpha}$. The catalytic activity of this sample was comparable to that of $Sr_{0.8}La_{0.2}Mn$

TABLE 3
Catalytic Activity of $Sr_{1-x}Ln_xMnAl_{11}O_{19-\alpha}$[a] for Methane Combustion

	$T_{10\%}$ (°C), $T_{90\%}$ (°C)[b]				
Ln	$x = 0$	$x = 0.2$	$x = 0.4$	$x = 0.6$	$x = 1.0$
Pr	550, 770	520, 770	520, 770	530, 770	520, 810
Nd	550, 770	520, 820	500, 770	520, 780	520, 770
Sm	550, 770	520, 770	520, 780	510, 780	570, 870
Gd	550, 770	530, 820	540, 780	520, 780	—, —

[a] All samples are calcined at 1200°C.
[b] Reaction conditions; CH_4 1 vol%, air 99 vol%, S. V. = 48,000 hr^{-1}.

$Al_{11}O_{19-\alpha}$, which was previously reported to be an active catalyst (13). In contrast, $T_{90\%}$ values of partially substituted samples were higher than that of unsubstituted sample. The decrease in catalytic activity in the high conversion level appears to correspond to small surface areas of the partially substituted samples. The differences in $T_{90\%}$ among various *Ln*-substituted samples with different x were also small.

In our previous report (13), the catalytic activity of the sample with *Ln* = La correlated well with its surface area. But clear correlation was unobservable in the present case. It is suggested that these results were due to the formation of the second phase in the substituted samples. La ions are easily dissolved into hexaaluminate lattice almost completely. In contrast, the essential surface area of hexaaluminate could be measured for the Ce-, Pr-, Nd-, Sm-, and Gd-substituted samples due to the precipitated second phase of $LnAlO_3$ or CeO_2.

Iyi *et al.* have reported that some hexaaluminate compounds contain Frenkel defects in the crystal lattice of β-alumina and magnetoplumbite structures (9, 17). The defective unit cell includes an interstitial Al^{3+} in the spinel block, an interstitial O^{2-}, and a vacancy of the large cation in the mirror plane. The defect concentration varies with a cation species in the mirror plane. Sr–hexaaluminate contains no Al^{3+} defect, whereas lanthanide (La or Nd)–hexaaluminate possesses 0.7 Al^{3+} defect per one unit cell (per 12 Al^{3+} site). Therefore, the defect concentration is greatly influenced by the cationic substitution. The oxidation state of the Mn ion or the amount of interstitial oxygen in the mirror plane compensates the charge of aliovalent cation. From the results of catalytic activities on CH_4 combustion (Table 3), it is supposed that observed improvements of catalytic activities for Ln-substituted hexaaluminate in the low-temperature region is closely related with both the concentration of the defect structure and the valence instability of the manganese ion.

CONCLUSIONS

In this study, $Sr_{1-x}Ln_xMnAl_{11}O_{19-\alpha}$ (*Ln* = Ce, Pr, Nd, Sm, or Gd) which have magnetoplumbite-type structure was prepared by using the alkoxide hydrolysis method. The crystalline phases and composition, specific surface areas, and catalytic properties for methane combustion were strongly influenced by the cationic substitution and are summarized as follows.

- Ce could be almost insoluble and existed as CeO_2.
- Two kinds of hexaaluminates (phase *A* and *B*), which are different in manganese content and unit cell size, coexisted in $SrMnAl_{11}O_{19-\alpha}$ ($x = 0$).
- Lanthanide cations, except for Ce, were preferentially substituted into phase *B* with a smaller lattice size than phase *A*. This substitution accompanied the increase of Mn concentration in the lattice.
- Pr, Nd, and Sm could be soluble even at $x = 1.0$ into a Sr site in mirror plane in the equilibrium state. However, partial precipitation of the impurity perovskite phase occurred simultaneously, which was promoted by substitution of *Ln* ions with different radius with that of Sr.
- Gd could be soluble into the hexaaluminate lattice at $0 < x \leq 0.6$.
- The hexaaluminate phase was retained after substituting Pr, Nd, Sm, or Gd for Sr; the catalytic activity for methane combustion was improved in the low-temperature region, which was supposed to be related with both the concentration of the defect structure and the oxidation state of Mn.

ACKNOWLEDGMENT

The present work was partially supported by the Grant-in-Aid for Scientific Research from the Ministry of Education, Japan.

REFERENCES

1. D. L. Trimm, *Appl. Catal.* **7,** 249 (1984).
2. R. Prasad, L. Kennedy, and E. Ruckenstein, *Catal. Rev. Sci. Eng.* **26,** 1 (1984).
3. H. Arai, *Hyomen* **24,** 658 (1986).
4. L. D. Prefferle and W. C. Prefferle, *Catal. Rev. Sci. Eng.* **29,** 219 (1987).
5. M. Machida, E. Eguchi, and H. Arai, *J. Catal.* **103,** 385 (1987).
6. A. L. N. Stevels and A. D. M. Schrama-de Pauw, *J. Electrochem. Soc.* **123,** 691 (1976).
7. J. M. P. J. Verstegen and A. L. N. Stevels, *J. Lumin.* **9,** 406 (1974).
8. A. L. N. Stevels and J. M. P. J. Verstegen, *J. Lumin.* **14,** 207 (1976).
9. N. Iyi, S. Takekawa, and S. Kimura, *J. Solid State Chem.* **83,** 8 (1989).
10. M. Machida, T. Shiomitsu, K. Eguchi, and H. Arai, *J. Solid State Chem.* **95,** 220 (1991).
11. M. Machida, T. Shiomitsu, T. Eguchi, and H. Arai, *J. Mater. Chem.* **2,** 455 (1992).
12. M. Machida, E. Eguchi, and H. Arai, *J. Catal.* **120,** 377 (1989).
13. M. Machida, E. Eguchi, and H. Arai, *J. Catal.* **123,** 477 (1990).
14. D. B. Williams, Ed., *in* "Practical Analytical Electron Microscopy in Materials Science," p. 67. VCH, Weinheim/New York, 1984.
15. T. Yamashita, A. Kato, N. Watanabe, and S. Matsuda, *Nippon Kagaku Kaishi* **9,** 1169 (1986).
16. R. S. Roth, J. R. Dennis, and H. F. Mcmurdie, *Phase Diagrams Ceram.* **6,** 136 (1987).
17. N. Iyi, Z. Inoue, S. Takekawa, and S. Kimura, *J. Solid State Chem.* **52,** 66 (1984).